



# Normal mode detection and splitting after Sumatra–Andaman earthquake

Mahmoud Abd El-Gelil<sup>a,\*</sup>, Spiros Pagiatakis<sup>b</sup>, Ahmed El-Rabbany<sup>c</sup>

<sup>a</sup> Geomatics Division, University of Cape Town, Cape Town, South Africa

<sup>b</sup> Department of Earth and Space Science, York University, Toronto, Canada

<sup>c</sup> Department of Civil Engineering, Ryerson University, Toronto, Canada

## ARTICLE INFO

### Article history:

Received 25 August 2009

Received in revised form 10 February 2010

Accepted 14 February 2010

### Keywords:

Superconducting gravimeter

Least squares spectrum

Normal mode

Earth free oscillations

## ABSTRACT

Apart from life loss and damages which earthquakes cause, their signature in the collected data either seismic and/or gravity enables us to define their location and dislocation (i.e., geometric parameters), time of occurrence, and magnitude. In addition, the Earth's interior physical parameters, such as density profile and anelasticity can be defined. Gravity data contribute additional knowledge about the Earth's interior through careful analyses of superconducting gravimeter (SG) records particularly after strong earthquakes. In this paper, SG data recorded after the Sumatra–Andaman earthquake in December 26, 2004 at eight SG stations, are used to investigate the properties of the long-period seismic modes: their frequencies, amplitudes, and quality factors. These parameters are estimated very precisely in this study for the spheroidal modes  ${}_0S_0$ ,  ${}_0S_2$  and  ${}_0S_3$ . In addition, for the first time we observe the toroidal modes  ${}_1T_4$  and  ${}_1T_5$ .

© 2010 Elsevier Ltd. All rights reserved.

## 1. Introduction and background

When an earthquake hits, the Earth is set to vibrations similar to a drum when it is hit (Alterman et al., 1974). The vibrations of the Earth after an earthquake event are called the Earth's free oscillations (EFO) or normal modes. Even though the gravity observation of the EFO is only two decades old, the theories used to define these modes have existed for more than a century (Masters and Widmer, 1995). There are more than one thousand modes that can be defined after strong earthquakes (with magnitude above 6.5). Each mode has its own frequency and quality factor, which depend on the structure of the Earth (Masters and Widmer, 1995). However, the interference between adjacent modes (in frequency) add difficulties in the estimation of their frequency and quality factor (Roult et al., 2006). These modes cause gravity variation and displacement on the Earth's surface which can be sensed by either gravimeters or seismometers.

The displacement at any point on the surface of the Earth due to the normal modes is relatively complicated. The total displacement is a combination of many discrete modes of oscillation each of which is characterized by a frequency and a quality factor. Similar to the total displacement, the total gravity change can be written as a sum of all decaying cosinusoid modes (Masters and Widmer,

1995):

$$g(t) = \sum_k A_k \cos(\omega_k t + \phi_k) e^{-\alpha_k t}, \quad (1)$$

where  $\omega_k$  is the frequency in rad/s of the  $k$ th mode which has an initial amplitude<sup>1</sup>  $A_k$  and initial phase  $\phi_k$ . The quality factor “ $Q$ ” of the  $k$ th mode can be estimated through its frequency  $\omega_k$  and the decay parameter  $\alpha_k$  (Masters and Widmer, 1995):

$$Q_k = \frac{\omega_k}{2\alpha_k}. \quad (2)$$

The larger the  $Q$ , the longer the period of time of the mode and vice-versa. There are modes with large  $Q$  that become excited and active for months and others with small  $Q$  stay for only days or hours. For an observed mode, its  $Q$  value can be estimated from the bandwidth of the peak or from the amplitude attenuation with time.

Recent research shows that the best SGs are stable and less noisy than seismometers for frequencies less than 1000  $\mu$  Hz (Rosat et al., 2004; Widmer-Schmidrig, 2003). The latest strong earthquakes in Peru (June 2001) and Sumatra–Andaman (December 2004) with moment magnitudes  $M_w = 8.4$  and 9.3, respectively, were sources of strong signals in the SG data, and thus allow the investigation of the EFO (Lei et al., 2005, 2007; Rosat et al., 2005). Detecting and estimating the frequencies of these modes and their quality factors provide additional constraints to the Earth models, while precise

\* Corresponding author. Tel.: +27 21 650 3569; fax: +27 21 650 3572.

E-mail addresses: [mahmoud.abdel-gelil@uct.ac.za](mailto:mahmoud.abdel-gelil@uct.ac.za) (M. Abd El-Gelil), [spiros@yorku.ca](mailto:spiros@yorku.ca) (S. Pagiatakis), [rabbany@ryerson.ca](mailto:rabbany@ryerson.ca) (A. El-Rabbany).

<sup>1</sup> This is the amplitude of the mode immediately after the earthquake and its value depends on the strength of the event.

**Table 1**  
GGP stations and their latitude, longitude and sampling interval used in this research to study the seismic normal modes.

Station	Country	Abbrev.	Instrument	Latitude	Longitude	Sampling interval (s)
Bad Homburg	Germany	H (1 and 2)	Dual sphere	50.2285 N	8.6113 E	5
Moxa	Germany	MO	Dual sphere	50.6450 N	11.6160 E	1
Wetzell	Germany	W (1 and 2)	Dual sphere	49.1440 N	12.8780 E	1
Medicina	Italy	MC	Compact	44.5219 N	11.6450 E	10
Strasbourg	France	ST	Compact	48.6217 N	7.6838 E	2
Vienna	Austria	VI	Compact	48.2493 N	16.3579 E	1
Canberra	Australia	CB	Compact	35.3206 S	149.0077 E	1
Sutherland	South Africa	S (1 and 2)	Dual sphere	32.3814 S	20.8109 E	1

estimation of the singlet frequencies improves the Earth density profile (Rosat et al., 2005).

Kamal and Mansinha (1992) used the SG data recorded at Cantley to study the EFO after the Minhasa Peninsula earthquake of April 1990 in the period 480–210 s, where modes from  ${}_0S_{13}$  to  ${}_0S_{40}$  exist. The low noise of the SG data and the magnitude of the Sumatra–Andaman Earthquake allowed Rosat et al. (2005) to use data recorded at eleven stations and clearly observe the splitting of  ${}_0S_2$  and  ${}_0S_3$ . In addition, for the first time they were able to observe the  ${}_2S_1$  without using the multistation technique. Roullet et al. (2006) did an extensive analysis of SG data collected after the two major earthquakes (Peru and Sumatra) to define the “Q” factor of  ${}_0S_0$ ,  ${}_0S_2$ ,  ${}_0S_3$  and  ${}_2S_1$  as well as their frequencies. According to Hu et al. (2006) and after introducing the wavelet method to remove the pressure effect from SG data, toroidal modes  ${}_1T_2$  and  ${}_1T_3$  could be observed unambiguously in the gravity records

## 2. The least squares spectrum revisited

The least squares spectral analysis (LSSA) has its roots in Vaníček (1969, 1971). Its advantages over classical Fourier analysis have already been presented earlier (see for example Craymer, 1998; Pagiatakis, 1999, 2000). In this section, the fundamental concepts and formulae of the LSSA are presented along with the associated statistical properties of the LS spectrum.

Consider a time series  $\mathbf{f}(\mathbf{t}_i)$  observed at discrete times  $\mathbf{t}_i$ ,  $i = 1, 2, \dots, \mathbf{n}$ , not necessarily evenly spaced, which is essentially equivalent to the presence of gaps in the time series. This time series is assumed to have an associated covariance matrix  $\mathbf{C}_f$  that carries information on the uncertainty of the observed values as well as on their correlation (usually not available). In spectral analysis, we use a set of orthogonal trigonometric base functions of cyclic frequency  $\omega_j$  to represent  $\mathbf{f}(\mathbf{t}_i)$ . Hence,  $\hat{\mathbf{P}}(\omega_j)$  which is the best fitting of the time series  $\mathbf{f}(\mathbf{t}_i)$  in the LS sense becomes:

$$\hat{\mathbf{P}}(\omega_j) = \hat{\mathbf{c}}_{1j} \cos(\omega_j \mathbf{t}) + \hat{\mathbf{c}}_{2j} \sin(\omega_j \mathbf{t}), \quad (3)$$

where  $\hat{\mathbf{c}}_{1j}$  and  $\hat{\mathbf{c}}_{2j}$  are the estimated coefficients from the least squares fitting of the base functions to the time series. The LSSA spectrum is described by the estimated percentage variance  $\hat{\mathbf{s}}(\omega_j)$  of the spectral content at the specific cyclic frequency  $\omega_j$ , which is the ratio of the quadratic norm of the specific signal to the total quadratic norm of the series:

$$\hat{\mathbf{s}}(\omega_j) = \frac{\mathbf{f}^T \mathbf{C}_f^{-1} \hat{\mathbf{P}}(\omega_j)}{\mathbf{f}^T \mathbf{C}_f^{-1} \mathbf{f}}, \quad \text{where } \mathbf{f}^T \mathbf{C}_f^{-1} \mathbf{f} \neq 0. \quad (4)$$

When  $\hat{\mathbf{P}}(\omega_j)$  fits  $\mathbf{f}(\mathbf{t}_i)$  perfectly, then  $\hat{\mathbf{s}}(\omega_j) = 1.0$ . On the other hand, it is possible that both  $\hat{\mathbf{c}}_{1j}$  and  $\hat{\mathbf{c}}_{2j}$  be zero, then  $\hat{\mathbf{s}}(\omega_j) = 0$ . Therefore,  $\hat{\mathbf{s}}(\omega_j) \in [0, 1]$ .

Pagiatakis (1999) showed that the probability density function (PDF) of the estimated LS spectrum  $\hat{\mathbf{s}}(\omega_j)$  is a *beta* distribution for known a priori variance factor while the PDF is a hypergeometric distribution for unknown a priori variance factor. However, the

two PDFs converge to the same distribution when the time series contains more than 150 data points. The *beta* distribution is used for the derivation of the PDF of the product spectrum since the length of time series used in this research is much longer than 150 points. This PDF is defined by two parameters  $\alpha$  and  $\beta$ , where  $\alpha=1$  and  $\beta$  depends on the number of data points (length of the time series) and the number of unknown parameters estimated by the LS estimation (degree of freedom of the LS system).

In general, defining the PDF of any random variable is very important for statistical testing. Spectral analysis is no exception, because the LS spectrum  $\hat{\mathbf{s}}(\omega_j)$  estimated from Eq. (4) is a random variable. Therefore, the *beta* distribution is always used to test the significance of the LS spectral peaks at a specific level of confidence (e.g., 90%, 95% and 99% CLs).

## 3. SG data and the Sumatra–Andaman earthquake

SG data pertaining to the Sumatra–Andaman earthquake were downloaded from the GGP database.<sup>2</sup> Only gravity and atmospheric pressure data are available. Unfortunately, the Cantley station was not operational at that time period. Stations used in this analysis are from the following countries: Australia (Canberra), Germany (Bad Homburg, Moxa and Wetzell), Italy (Medicina), South Africa (Sutherland), France (Strasbourg) and Austria (Vienna) (see Table 1 for more details about these stations). There are four stations with dual sphere instruments while the other four are compact SG with single sphere. The majority of the SG stations are in Europe. However there are two stations in the southern hemisphere (CB, S1 and S2). Number “1” in the abbreviation (e.g., S1) refers to the lower sphere while number “2” (e.g., S2) refers to the upper sphere. Moxa station has a dual sphere instrument but only the lower sphere records are available from the GGP database.

There are two months of SG data from all stations starting on December 1, 2004. The Sumatra–Andaman earthquake occurred on December 26, 2004. There are 26 days before the occurrence of the earthquake and 34 days after. Data recorded before the earthquake are quiet i.e., they do not include any EFO signals. In this study we determine the atmospheric pressure admittance for each station independently in order to correct the data before we do the analysis of the normal modes. To estimate the pressure admittance, only data before the earthquake are considered and we follow the least squares response method (LSRM) developed in Abd El-Gelil et al. (2008).

## 4. Frequency dependent pressure admittance

To avoid the effect of the earthquake (i.e., EFO signals), only 540.0 h of data recorded before the earthquake are used. We follow

<sup>2</sup> GGP data centre was located at the International Centre for Earth Tides (ICET) in Brussels, Belgium (<http://www.eas.slu.edu/GGP/>). As of January 2008, ICET operations were transferred to Tahiti, French Polynesia.

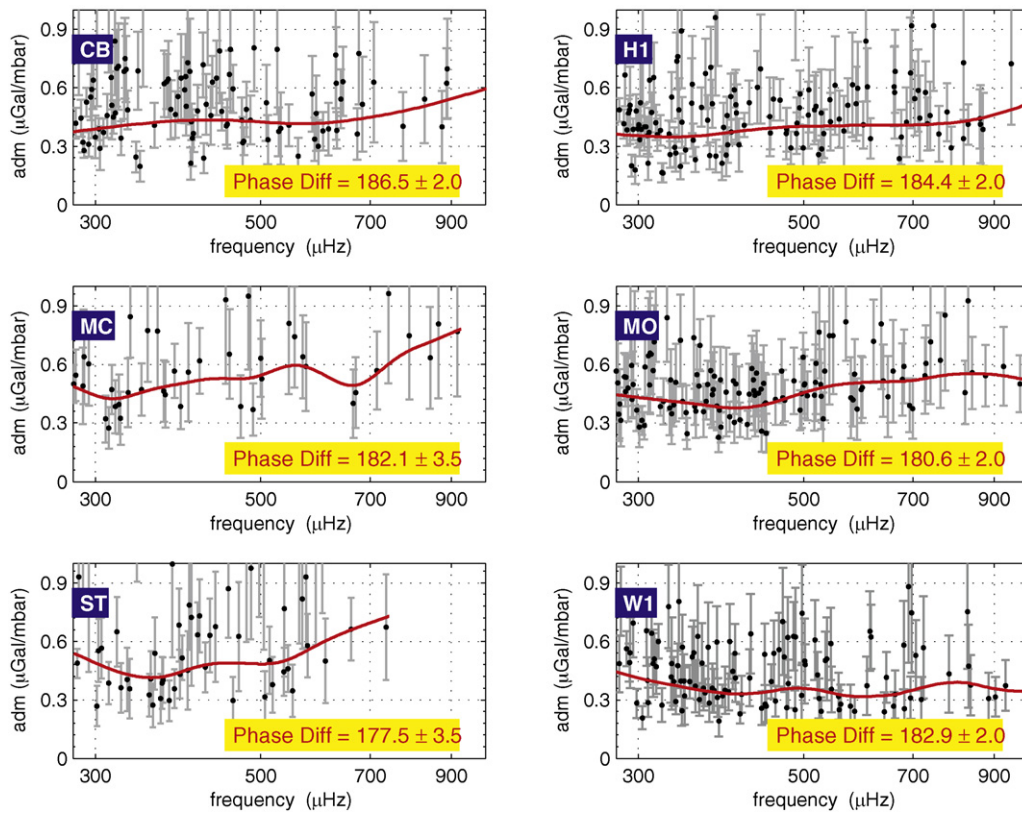


**Fig. 1.** The atmospheric pressure admittance of six stations used in this study. Phase differences are weighted averages. Station code names are as follows: CB (Canberra), H1 (Bad Homburg, lower sphere), MC (Medicina), MO (Moxa, lower sphere), ST (Strasbourg) and W1 (Wetzlar, lower sphere).

the same steps as in Abd El-Gelil et al. (2008) to estimate the frequency dependent pressure admittance for each station based on the LSRM. In other words, the Earth and ocean loading tides are removed first. Then, both gravity residuals and pressure data are filtered using a bandpass filter from a combination of Parzen algorithms with a passband 150–14,900  $\mu\text{Hz}$ . As in LSRM, common peaks in both gravity and pressure are used to estimate the admittance. Fig. 1 shows the admittances (amplitude and phase) of six stations used in this study. It is obvious that the estimated admittance is frequency- and location-dependent. Gravity has a high correlation with the pressure in the frequency lower than 1500  $\mu\text{Hz}$  (Hu et al., 2006). Hence, we estimate the frequency-dependent admittance in the frequency band 200–1050  $\mu\text{Hz}$ . Accurate atmospheric pressure admittance can be determined by fitting a cubic spline to the scattered amplitudes in Fig. 1. The weighted average is used for each station to estimate the phase difference of the admittance. Most of the phase differences are close to  $180.0^\circ$ .

It is well known indeed that the pressure admittance is always negative for gravity. Its nominal value of  $-0.300 \mu\text{Gal/mbar}$  results from the superposition of the direct upward attraction of the air masses, which is close to  $-0.400 \mu\text{Gal/mbar}$ , and the gravity increase associated with the ground subsidence under the weight of these masses. This compensation reaches  $+0.100 \mu\text{Gal/mbar}$  when it is complete. The range of the amplitude of the admittance that we observe ranges from  $-0.355$  to  $-0.750 \mu\text{Gal/mbar}$ . The difference with the nominal value can be due to different factors. First of all, the compensation due to the ground subsidence is effective only for long period pressure effects associated with large pressure cells, as it is the case in the tidal bands. For periods below 1 h (frequencies higher than 280  $\mu\text{Hz}$ ) the size of the pressure cells becomes too small to effectively depress the ground surface and values up to  $-0.400 \mu\text{Gal/mbar}$  can be observed. Moreover higher SG noise level could be absorbed by the pressure admittance.

To remove the pressure effect from the gravity data after the Earthquake, the pressure is transformed into the frequency domain using Fourier transform. Next, the frequency-dependent admittance of each station is multiplied by the pressure in the frequency domain (frequency domain multiplication) and the output is transformed to the time domain using inverse Fourier transform and then removed from the gravity data. Now, the gravity data are free from all the known signals and can be used to investigate the EFO.

## 5. Earth free oscillations-EFO

The displacement of a point, with respect to the center of the mass of the Earth, can follow either a spheroidal or toroidal vibrational pattern. The spheroidal mode is denoted as  $nS_\ell$  while  $nT_\ell$  is the notation of the toroidal mode. Here,  $n$  is the number of nodes between the center of the mass of the Earth and its surface for a radial wave function of a mode, while integer  $\ell$  is the angular degree describing the horizontal structure of motions associated with the mode.  $n = 0$  corresponds to the lowest frequency “fundamental modes.” Due to Earth rotation, ellipticity, and lateral inhomogeneity, each mode (e.g.,  $nS_\ell$ ) is split into  $2\ell + 1$  number singlets (Masters and Widmer, 1995). Each singlet can be represented as  $nS_\ell^m$  where  $m \in [-\ell, \ell]$ . For example, the  $0S_2$  mode has five singlets ( $0S_2^{-2}$ ,  $0S_2^{-1}$ ,  $0S_2^0$ ,  $0S_2^{+1}$  and  $0S_2^{+2}$ ) from low to high frequency. Also, the Earth rotation and ellipticity cause the toroidal modes to be observed in the gravity records even though they do not have a radial component. This is due to the coupling between the spheroidal and toroidal modes as a result of the Coriolis force (Zürn et al., 2000).

### 5.1. Spheroidal modes

A selected set of spheroidal modes is presented with their amplitudes, splitting and  $Q$ . The first one is the  $0S_0$  mode, which is called

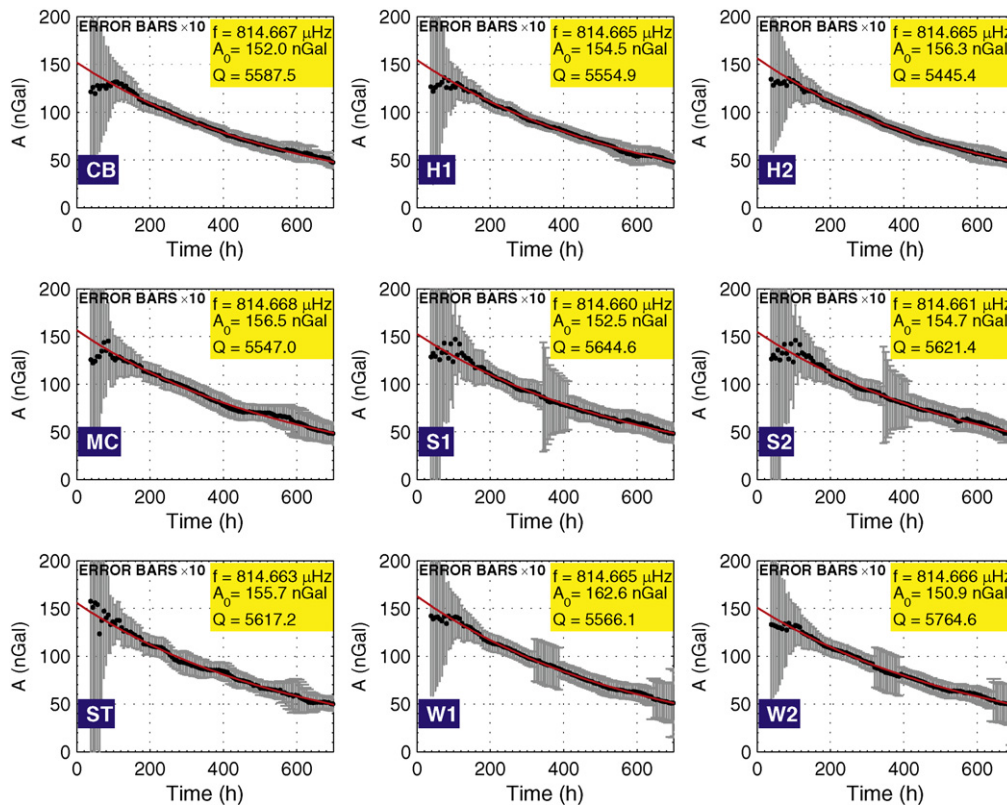


**Fig. 2.** Estimation of the quality factor “ $Q$ ” from amplitude fitting of 75.0 h window with 6.0 h shift in time ( $x$ -axis) from the onset of the earthquake. Stations are as follows; CB (Canberra), H1 and H2 (Bad Homburg), MC (Medicina), S1 and S2 (Sutherland), ST (Strasbourg) and W1 and W2 (Wetzell).

the “breathing mode” of the Earth. It has only a radial displacement component (compression and dilatation) with a period of 20.5 min (Dziewonski and Anderson, 1981). The Sumatra–Andaman earthquake excited this mode very strongly. It can be observed easily by all SGs with amplitude of more than 4 nGal on average, and for longer than three months. At each station, the frequency of  ${}_0S_0$  has been estimated by fitting a Lorentzian function<sup>3</sup> to the LS spectrum associated with the standard deviation of the fitting (Dahlen and Tromp, 1998). Worth mentioning here is that the standard deviation of the estimated frequencies represent the uncertainties with respect to the fitting function and not related to the frequency resolution. The weighted average of these estimated frequencies for the 11 datasets (from eight stations) is  $814.6657 \pm 0.7 \times 10^{-3} \mu\text{Hz}$  with negligible difference from PREM model which is  $814.6639 \mu\text{Hz}$ .

To find the initial amplitude and the quality factor “ $Q$ ”, the gravity residual time series are segmented arbitrarily into 75.0 h length segments with a 6.0 h sliding (moving) window (Hu et al., 2006; Roult et al., 2006). Then, the weighted least squares is used to estimate the amplitude at the center of each segment along with its standard error. Fig. 2 shows these amplitudes and their error bars. Then, the decay parameter  $\alpha$  is estimated by fitting an exponential function based on the weighted LS principle, which can lead to the calculation of  $Q$  by applying Eq. (1). The quality factor is estimated at each station and the weighted average of  $5551.0 \pm 9.1$  is obtained which is higher than the PREM value of 5327 (Dziewonski and Anderson, 1981). The same data set was used by Rosat et al. (2005) and they found  $Q = 5506 \pm 19$  which is closer to our estimated value here but it is less precise.

Two concluding points: (1) our estimation of the  ${}_0S_0$  initial amplitude does not show an obvious variation among all stations. The average amplitude is  $155.4 \pm 0.2$  nGal. However, the SG at Wetzell, Germany shows more than 10 nGal difference between the upper and lower spheres, which may be the result of mis-calibration. Other dual sphere units are consistent and within the allowance of the calibration error (0.1%) and (2) it is important to use the standard errors (error bars in Fig. 2) for the initial amplitude estimation because the SG data scatter immediately after the earthquake is much higher than later.

The second spheroidal mode is called the “football mode” and is represented by  ${}_0S_2$ . It has five singlets and all of them are clearly excited after the earthquake. Fig. 3 shows these singlets above the noise level at all stations. In fact, all singlets are visible in the spectra of the northern hemisphere stations specially the central one. Table 2 presents the frequency and the  $Q$  of each singlet along with their standard error. Unlike the spectra of the northern hemisphere stations, we can notice that the middle singlets  ${}_0S_2^{-1}$ ,  ${}_0S_2^0$  and  ${}_0S_2^{+1}$  in the spectra of the southern hemisphere are obscured in the noise and they can barely be observed. This low signal-to-noise ratio may be explained by the fact that the latitudes of the two stations are very close to the nodal line of the degree two spheroidal harmonic ( $35.26^\circ\text{S}$ ).

The third spheroidal mode is  ${}_0S_3$ . Fig. 4 shows the splitting of the  ${}_0S_3$  with average quality factor  $426.4 \pm 6.6$  while the PREM model gives 417.54. The singlets of this mode are clearly visible in most SG data. Table 2 presents the frequency and the  $Q$  of each singlet. Comparisons with the PREM model and with the latest and most comprehensive study (Roult et al., 2006) are also included in Table 2.

The last spheroidal mode presented in this section is the  ${}_2S_1$ . It is the first overtone of the Slichter mode. It was first identified in the SG records after the Peru earthquake, June 2001 (Rosat et al., 2005). In fact, not all the singlets of this mode were excited. Most SG

<sup>3</sup> The Lorentzian function is the singly peaked function which gives the shape of certain types of spectral lines. For more details about this function, readers can see <http://mathworld.wolfram.com/LorentzianFunction.html>.

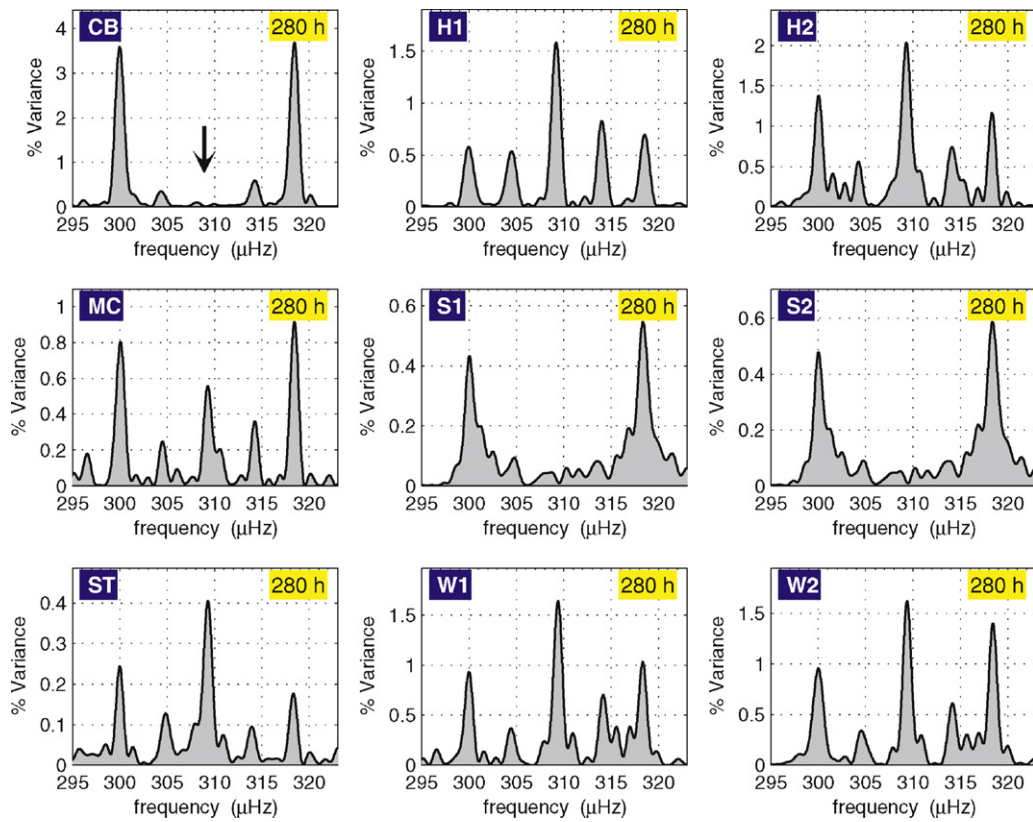


**Fig. 3.** Mode  ${}_0S_2$  and its singlets from 280.0 h data length after the earthquake. Stations are as follows: CB (Canberra), H1 and H2 (Bad Homburg), MC (Medicina), S1 and S2 (Sutherland), ST (Strasbourg) and W1 and W2 (Wetzell).

**Table 2**  
Spheroidal modes with their frequencies and Q compared with PREM and Roullet et al. (2006).

Mode	$\ell$	PREM		Roullet et al. (2006)		This study	
		$f(\mu\text{Hz})$	Q	$f(\mu\text{Hz})$	Q	$f(\mu\text{Hz})$	Q
${}_0S_0$		814.6639	5500	$814.661 \pm 0.005$	$5489.1 \pm 19.0$	$814.666 \pm 0.7 \times 10^{-3}$	$5551.0 \pm 9.1$
	-2	300.001	494.6	$299.779 \pm 0.074$	$490.6 \pm 14.0$	$300.001 \pm 1.2 \times 10^{-3}$	$509.9 \pm 3.9$
	-1	304.493	501.8	$304.624 \pm 0.029$	$562.9 \pm 4.0$	$304.533 \pm 1.1 \times 10^{-3}$	$677.9 \pm 11.5$
${}_0S_2$	0	309.064	509.3	$309.397 \pm 0.157$	$395.6 \pm 11.3$	$309.296 \pm 1.1 \times 10^{-3}$	$512.3 \pm 3.9$
	1	313.716	517.0	$313.892 \pm 0.069$	$495.3 \pm 4.0$	$313.882 \pm 0.5 \times 10^{-3}$	$592.7 \pm 8.1$
	2	318.452	524.0	$318.465 \pm 0.089$	$480.2 \pm 14.9$	$318.402 \pm 1.0 \times 10^{-3}$	$520.3 \pm 3.1$
	-3	461.986	411.7	$461.646 \pm 0.087$	$450.5 \pm 63.3$	$461.662 \pm 0.4 \times 10^{-3}$	$393.2 \pm 8.2$
	-2	464.123	413.6	$464.329 \pm 0.071$	$442.5 \pm 46.3$	$464.377 \pm 0.5 \times 10^{-3}$	$474.5 \pm 24.7$
${}_0S_3$	-1	466.272	415.5	$466.236 \pm 0.083$	$456.6 \pm 93.0$	$466.121 \pm 0.2 \times 10^{-3}$	$466.6 \pm 25.6$
	0	468.433	417.4	$468.560 \pm 0.042$	$434.2 \pm 19.3$	$468.456 \pm 0.2 \times 10^{-3}$	$468.5 \pm 18.4$
	1	470.606	419.3	$470.877 \pm 0.052$	$339.9 \pm 68.9$	$470.920 \pm 0.3 \times 10^{-3}$	$501.5 \pm 32.4$
	2	472.791	421.3	$472.659 \pm 0.133$	$493.9 \pm 56.3$	$472.505 \pm 0.7 \times 10^{-3}$	$573.4 \pm 41.5$
	3	474.989	423.3	$474.269 \pm 0.468$	$382.6 \pm 39.2$	$474.535 \pm 2.1 \times 10^{-3}$	$605.3 \pm 49.4$

stations show clearly the  ${}_2S_1^{+1}$  singlet after the Sumatra–Andaman earthquake, December 2004. It is statistically significant above 95% CL while the other singlets are either buried in the noise or not excited. Fig. 5 shows this mode at four SG stations.

**Table 3**  
Toroidal modes observed in this study and compared with the PREM and Hu et al. (2006).

	Toroidal modes $f(\mu\text{Hz})$				
	${}_0T_2$	${}_0T_3$	${}_0T_4$	${}_1T_4$	${}_1T_5$
This study	377.60	586.90	764.60	1586.3	1749.9
PREM	379.17	586.16	765.66	1585.50	1750.50
Hu et al. (2006)	378.23	586.34	765.86	–	–

### 5.2. Toroidal modes

In general, the toroidal modes are difficult to observe in the gravity records. However, coupling between spheroidal and toroidal modes due to the Earth's ellipticity and rotation causes the toroidal modes to appear on the gravimeter records. In this research, we could identify nine of these modes as seen in Fig. 6 at CL higher than 95%.  ${}_0T_2$ ,  ${}_0T_3$  and  ${}_0T_4$  are observed at 377.60, 586.90 and 764.60  $\mu\text{Hz}$ , respectively, which are similar to what Hu et al. (2006) estimated. Only the  ${}_0T_4$  frequency is smaller by more than 1.0  $\mu\text{Hz}$  while other discrepancies are not significant (Table 3). Modes  ${}_1T_4$  and  ${}_1T_5$  are observed here for the first time with frequencies 1586.3 and 1749.9  $\mu\text{Hz}$ , respectively. This new observation demonstrates the power and effectiveness of the developed methodology to filter and clean the data from the noise, especially the frequency depen-

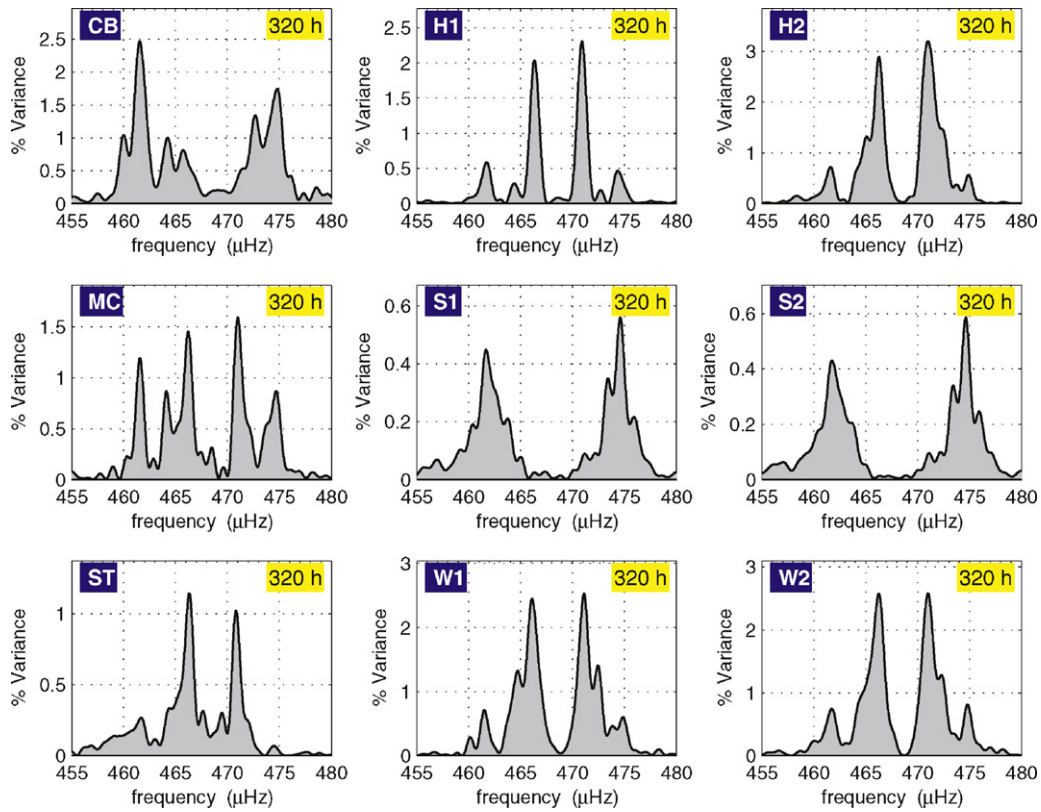


**Fig. 4.** Mode  $0S_3$  and its singlets from 320.0 h data length after the earthquake. Stations are as follows: CB (Canberra), H1 and H2 (Bad Homburg), MC (Medicina), S1 and S2 (Sutherland), ST (Strasbourg) and W1 and W2 (Wetzfel).

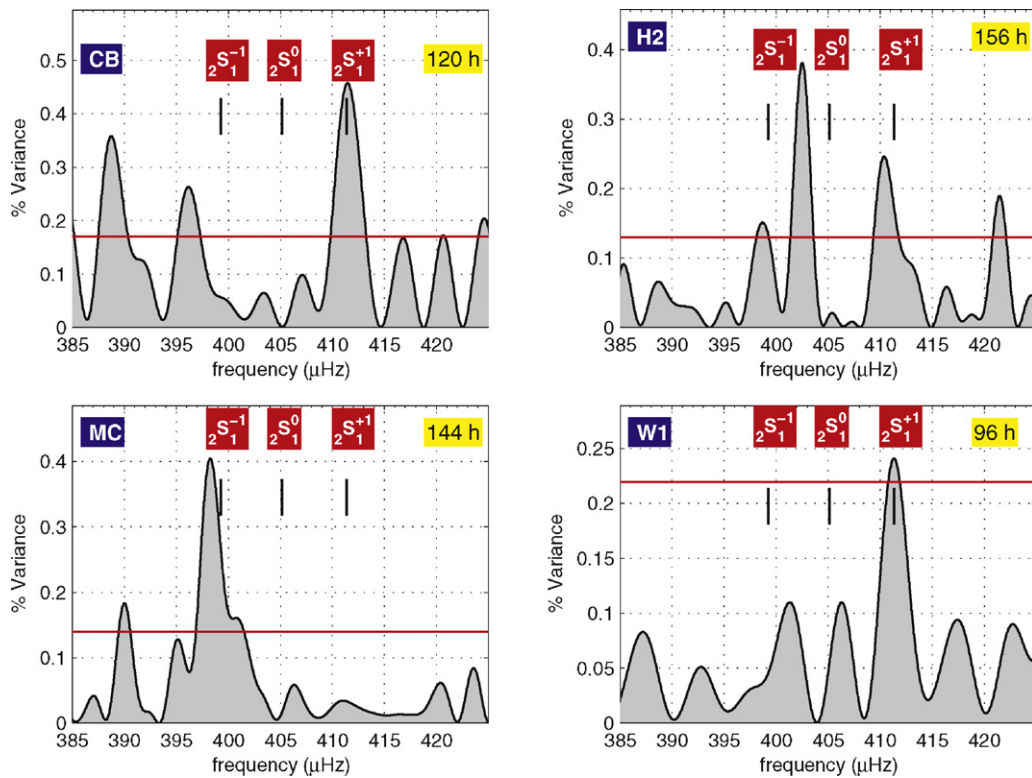


**Fig. 5.** Mode  $2S_1$  and its singlets. Stations are as follows: CB (Canberra), H2 (Bad Homburg), MC (Medicina) and W1 (Wetzfel) with different data length (shown on the upper right corner of each panel).

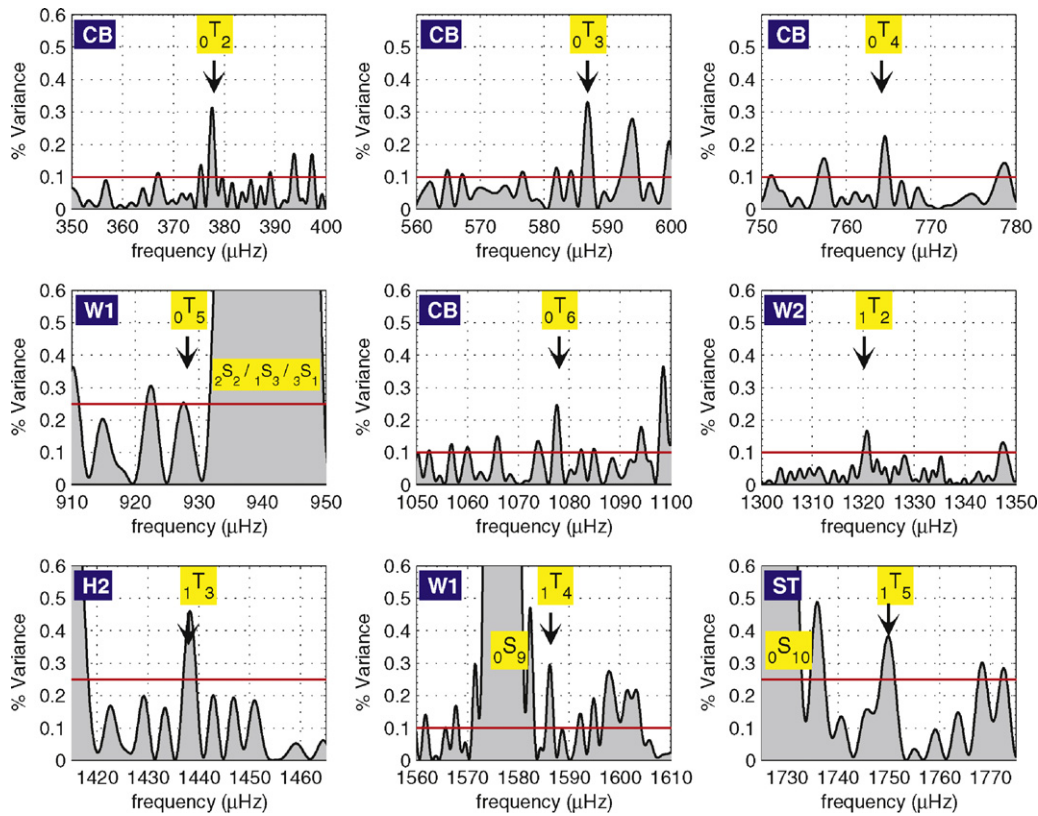


Fig. 6. Toroidal modes. The solid line shows the 95% CL while the downward arrows identify the main mode.

dent admittance. This opens the door to the researchers to detect and identify the seismic normal mode (toroidal) not only for frequencies lower than 1500  $\mu$  Hz but also for higher frequencies (e.g.,  $1T_4$  and  $1T_5$ ).

## 6. Concluding remarks and discussion

By analysing the SGs data after the Sumatra–Andaman earthquake, the following remarks can be made:

1. New toroidal modes namely  $1T_4$  and  $1T_5$  could be identified for the first time which reveal the effectiveness of the procedure developed and applied in this research. This includes the frequency dependent admittance, the filtering algorithm and over all the applicability of the LSSA as a spectral analysis method.
2. Latitude dependence of  $0S_0$  could not be verified by this study because most of the stations are close to mid-latitude and there is no station close to the equator or the poles.
3. Most of the estimated  $Q$  values based on the SG data are larger than the predicted  $Q$  from PREM model. These modes are ringing for long time, longer than PREM predict i.e., they take long time to be attenuated.
4. For Dual sphere instruments, it is very important to use a sound calibration method for both spheres, otherwise discrepancies may exist in the records of the same signal. The LS spectrum of the spheroidal modes of S1 and S2 and W1 and W2 are almost identical while for H1 and H2 are not. It is obvious that the splitting can be seen in H1 for a specific data length, while H2 fuses the singlets together for most of the modes. Also, H1 is less sensitive than H2, because for the same data length the LS spectrum of H1 has less power than H2. This may be due to manufacturing differences.

5. For stations in Europe, even though they are close to one other, only a few singlets are clearly visible in a subset of stations and hidden in others (e.g.,  $2S_1^+$  is visible in all stations except in Medicina (MC) where  $2S_1^-$  is the only visible peak).
6. The results presented herein are more precise than the ones from previous work by Rosat et al. (2005) and have smaller standard error for  $Q$  and singlet frequencies than in Roult et al. (2006).

## Acknowledgments

This research was financially supported by Ryerson University Post Doctoral Fellowship for the first author and the Natural Sciences and Engineering Research Council (NSERC) of Canada, the GEOIDE National Centre of Excellence of the second and third authors. We thank the managers of the GGP stations for making the SG data available for this research. The first anonymous reviewer and Professor Sun Heping provided very useful comments and suggestions that improved significantly the manuscript.

## References

- Abd El-Gelil, M., Pagiatakis, S., El-Rabbany, A., 2008. Frequency-dependent atmospheric pressure admittance of superconducting gravimeter records using least squares response method. *Phys. Earth Planet. Inter.* 170, 24–33.
- Alterman, Z., Eyal, Y., Merzer, A., 1974. On free oscillations of the Earth. *Geophys. Surv.* 1, 409–428.
- Craymer, M., 1998. The Least Squares Spectrum, its Inverse Transform and Autocorrelation Function: Theory and Some Applications in Geodesy. Ph.D. Thesis. University of Toronto, Canada.
- Dahlen, F., Tromp, J., 1998. *Theoretical Global Seismology*. Princeton University Press, Princeton, NJ.
- Dziewonski, A., Anderson, D., 1981. Preliminary reference earth model. *Phys. Earth Planet. Int.* 25, 297–356.
- Hu, X., Liu, L., Hinderer, J., Sun, H., 2006. Wavelet filter analysis of atmospheric pressure effects in the long-period seismic mode band. *Phys. Earth Planet. Inter.* 154 (1), 70–84.

- Kamal, Mansinha, L., 1992. A test of the superconducting gravimeter as a long-period seismometer. *Phys. Earth Planet. Inter.* 71, 52–60.
- Lei, X., Xu, H., Sun, H., 2005. Detection of spheroidal free oscillation excited by Peru 8.2 M<sub>s</sub> earthquake with five international superconducting gravimeter data. *Sci. China Ser. D: Earth Sci.* 48 (1), 123–133.
- Lei, X., Sun, H., Hsu, H., Shi, Y., 2007. Check of Earth's free oscillation excited by Sumatra–Andaman large earthquake and discussions on the anisotropy on inner core. *Sci. China Ser. D: Earth Sci.* 50 (6), 909–917.
- Masters, G., Widmer, R., 1995. Free oscillation: frequencies and attenuations. *Global Earth Physics, A Handbook of Physical Constants*, AGU Reference Shelf 1.
- Pagiatakis, S., 1999. Stochastic significance of peaks in the least-squares spectrum. *J. Geodesy* 73, 67–78.
- Pagiatakis, S., 2000. Application of the Least-squares Spectral Analysis to Superconducting Gravimeter Data Treatment and Analysis: Proceedings of the Workshop on High Precision Gravity Measurements with Application to Geodynamics and Second GGP Workshop, Cahiers Du Centre Europeen De Geodynamique et de Seismologie (ECGS), 17, pp. 103–113.
- Rosat, S., Hinderer, J., Crossley, D., Boy, J., 2004. Performance of superconducting gravimeters from long-period seismology to tides. *J. Geodyn.* 38, 461–476.
- Rosat, S., Sato, T., Imanishi, Y., Hinderer, J., Tamura, Y., McQueen, H., Ohashi, M., 2005. High-resolution analysis of the gravest seismic normal modes after the 2004 Mw = 9 Sumatra earthquake using superconducting gravimeter data. *Geophys. Res. Lett.* 32, L13304.
- Roult, G., Rosat, S., Millot-Langet, R., Clévéché, E., Hinderer, J., 2006. New determinations of *Q* quality factors and eigenfrequencies for the whole set of singlets of the Earth's normal modes  ${}_0S_0$ ,  ${}_0S_2$ ,  ${}_0S_3$  and  ${}_2S_1$  using SG data from the GGP network. *J. Geodyn.* 41 (1–3), 345–356.
- Vaniček, P., 1969. Approximate spectral analysis by least-squares fit. *Astrophys. Space Sci.* 4, 387–391.
- Vaniček, P., 1971. Further development and properties of the spectral analysis by least-squares. *Astrophys. Space Sci.* 12, 10–33.
- Widmer-Schmidrig, R., 2003. What can superconducting gravimeters contribute to normal mode seismology. *Bull. Seis. Soc. Am.* 93 (3), 1370–1380.
- Zürn, W., Laske, G., Widmer-Schmidrig, R., Gilbert, F., 2000. Observation of Coriolis coupled modes below 1 mHz. *Geophys. J. Int.* 143, 113–118.